

Band Structure and Pairing Nature of $\text{La}_3\text{Ni}_2\text{O}_7$ Thin Film at Ambient Pressure

Zhi-Yan Shao,^{1,*} Yu-Bo Liu,^{2,*} Min Liu,^{3,†} and Fan Yang^{1,‡}

¹*School of Physics, Beijing Institute of Technology, Beijing 100081, China*

²*Institute of Theoretical Physics, Beijing 100080, China*

³*College of Mathematics and Physics, Beijing University of Chemical Technology, Beijing 100029, China*

Recently, evidences of superconductivity with onset temperature T_c above the McMillan limit (≈ 40 K) have been detected in the $\text{La}_3\text{Ni}_2\text{O}_7$ ultrathin film grown on the LaSrAlO substrate at ambient pressure. This progress makes it possible to investigate the pairing mechanism in the bilayer nickelates through adopting various experimental tools. Here we perform a first-principle density-functional-theory (DFT) based calculation for the band structure of this nickelate superconductor. The obtained band structure is different from that of the pressurized bulk $\text{La}_3\text{Ni}_2\text{O}_7$ mainly in that the bonding- d_{z^2} band is pushed far (≈ 0.16 eV) below the Fermi level. Taking the low-energy Ni- ($3d_{z^2}, 3d_{x^2-y^2}$) orbitals placed on the pseudo-tetragonal lattice structure, we construct a 2D bilayer eight-band tight-binding model which well captures the main features of the DFT band structure. Then considering the multi-orbital Hubbard interaction, we adopt the random-phase approximation approach to investigate the pairing symmetry. The obtained spin susceptibility is maximized at the momentum $\mathbf{Q} = (0, \pm 0.86\pi)$ in the folded Brillouin zone, induced by Fermi-surface nesting, leading to interlayer antiferromagnetic spin fluctuation in the diagonal double-stripe pattern similar with that reported for the bulk $\text{La}_3\text{Ni}_2\text{O}_7$. The leading and subleading pairing symmetries are the s^\pm and approximate d_{xy} , which are nearly degenerate. Our results appeal for experimental verifications.

Introduction: The discovery of high-temperature superconductivity (SC) in the Ruddlesden-Popper (RP) phase multilayer nickelate superconductors $\text{La}_3\text{Ni}_2\text{O}_7$ [1] and $\text{La}_4\text{Ni}_3\text{O}_{10}$ [2–5] under high pressure (HP) has aroused a surge in the exploration of the pairing mechanism and physical properties of the nickelates family both experimentally [6–24] and theoretically [25–84]. As a new platform to study the high-temperature SC, the nickelates family is different from the cuprates and the iron-based superconductors family mainly in the aspect of the strong interlayer coupling in this family, which might play a crucial role in the pairing mechanism [25–46]. Previously, the SC in these RP phase nickelates only emerges under HP, while most experiments can only be conducted at ambient pressure (AP) due to technical difficulties. This strongly hinders the experimental investigation of the pairing mechanism of the materials. Very recently, this research field witnessed a breakthrough, i.e. the detection of SC with T_c above the McMillan limit (≈ 40 K) in the $\text{La}_3\text{Ni}_2\text{O}_7$ [85] and $\text{La}_{2.85}\text{Pr}_{0.15}\text{Ni}_2\text{O}_7$ [86] thin films grown on the LaSrAlO (LSAO) substrate at AP by two different teams independently.

The nickelate thin films synthesized by both teams exhibit similar onset $T_c \sim 42 - 45$ K of the superconducting transition in the temperature-dependent resistivity $\rho(T)$. While zero resistivity is observed by both teams, the corresponding temperature (9 K) for the $\text{La}_{2.85}\text{Pr}_{0.15}\text{Ni}_2\text{O}_7$ [86] film is higher than that (2 K) for the $\text{La}_3\text{Ni}_2\text{O}_7$ [85] film, possibly because the substitutions of Pr for La effectively inhibits the intergrowth of different RP phases [9], resulting in a nearly pure bilayer structure in the thin film. This fact implies that the nickelates accounting for the SC in the synthesized film is really in the 327 phase. Clear Meissner effect reflected by

the diamagnetic susceptibility has been detected by both teams through using the mutual-inductance technique. While the combined zero resistivity and Meissner effect unambiguously identify the SC, the Brezinskii-Kosterlitz-Thouless (BKT) transition revealed by the nonlinear voltage-current relation near the zero-resistivity temperature [85] and the distinct temperature-dependent behaviors of the in-plane and out-of-plane critical magnetic fields [86] reveal the 2D characteristic of the SC. Furthermore, through tuning the strength of the strain, it is found that higher T_c is correlated with smaller in-plane lattice constant [85]. Currently, the electronic structure and pairing mechanism of this material remain unknown.

In this paper, we construct a Ni- ($3d_{z^2}, 3d_{x^2-y^2}$) orbital tight-binding (TB) model to investigate the pairing symmetry for the $\text{La}_3\text{Ni}_2\text{O}_7$ film grown on the LSAO substrate. Our density-functional-theory (DFT) band structure shows that the low-energy degrees of freedom are dominated by the Ni- $3d_{z^2}$ and $3d_{x^2-y^2}$ orbitals, and the bonding- d_{z^2} band top is considerably far (≈ 0.16 eV) below the Fermi level. Using the two Ni- $3d-e_g$ orbitals placed in the pseudo-tetragonal A_{1g} structure, we construct a 2D eight-band TB model, which well fits the DFT band structure. After considering the multi-orbital Hubbard interactions, we engage the random-phase-approximation (RPA) approach to investigate the pairing symmetry. The RPA results show that the spin susceptibility is maximized at $\mathbf{Q} = (0, \pm 0.86\pi)$, which is just the nesting vector between the electron pocket centering around the Γ -point and the hole pocket centering around the $X_1(0, \pi)$ -point in the folded Brillouin zone (BZ). The obtained leading and subleading pairing symmetries are s^\pm and approximate d_{xy} respectively, which are nearly degenerate. Such near degeneracy is caused

by the reduced in-plane lattice constants and the enhanced c -axis one which benefits the intraplayer pairing d_{xy} -symmetry. In comparison with the pressurized bulk $\text{La}_3\text{Ni}_2\text{O}_7$, the T_c obtained here is lower, due to lack of the γ -pocket at the bonding- d_{z^2} band top. Our results appeal for experimental verification.

DFT Band Structure: The ultrathin film of $\text{La}_3\text{Ni}_2\text{O}_7$ crystallizes in a pseudo-tetragonal phase at AP, as seen in Fig. 1(a). The NiO_6 octahedron layers were separated by La-O layers along the c -axis. First-principles DFT calculations were implemented utilizing the Vienna ab initio simulation package (VASP) and employing the projector augmented wave (PAW) as the pseudopotentials [87–89]. The electronic correlations were considered by the generalized gradient approximation (GGA) and the Perdew-Burke-Ernzerhof (PBE) exchange potential [90]. The plane-wave cutoff energy was set as 550 eV and a k -point grid $12 \times 12 \times 3$ was adopted for the conventional structure of $\text{La}_3\text{Ni}_2\text{O}_7$ in *Amam* phase. We adopted the experimental lattice parameters of $\text{La}_{2.85}\text{Pr}_{0.15}\text{Ni}_2\text{O}_7$ with $a = b = 5.3033 \text{ \AA}$ and $c = 20.74 \text{ \AA}$ [86]. The internal coordinates are optimized until the atomic forces become less than 10^{-4} eV/\AA . The optimized spacing between two adjacent Ni-O planes is 4.11 Å, which is in well agreement with the experimental value (4.09 Å). The calculated Ni-O-Ni angle between two adjacent octahedra is 172.4° , which is a little bigger than the bulk one with the value of 168° . We performed DFT+ U band calculations with the onsite Coulomb interaction $U = 3.5 \text{ eV}$, which are reasonable value for this system[1, 22].

Along the high-symmetric lines exhibited in the folded BZ corresponding to the doubled unit cell shown in Fig. 1(b), we present our DFT+ U band structure in Fig. 1(c). The orbital weight distribution shown in Fig. 1(c) suggests that the electronic states near the Fermi level are primarily derived from Ni- $d_{x^2-y^2}$ and Ni- d_{z^2} orbitals, as is also verified in the orbital-dependent density of state (DOS) shown in Fig. 1(d). The Ni- d_{z^2} bands have a flat dispersion along the path of Γ -X and S- Γ -Y, which means the Ni- d_{z^2} band in the in-plane has a weak hybridization with the O- p orbitals. Owing to the strong interlayer coupling through the Ni- d_{z^2} and O- p_z orbitals, the Ni- d_{z^2} bands split into the bonding and antibonding states at Γ point. Consequently, the bonding d_{z^2} band top is pushed below the Fermi level by 0.16 eV, different from the situation in the pressurized bulk $\text{La}_3\text{Ni}_2\text{O}_7$ wherein the top of this band crosses the Fermi level and form a hole pocket [48]. This feature suggests that the metallization of the bonding- d_{z^2} band [1] is not necessary for the SC in $\text{La}_3\text{Ni}_2\text{O}_7$.

For convenience in the succeeding studies, we construct a Wannier model with the Ni- $d_{x^2-y^2}$ and Ni- d_{z^2} orbitals based on the maximally-localized Wannier function method implemented in the WANNIER90 code [91]. The hopping parameters in the TB model are obtained by Wannier downfolding the band structure with Ni- $d_{x^2-y^2}$

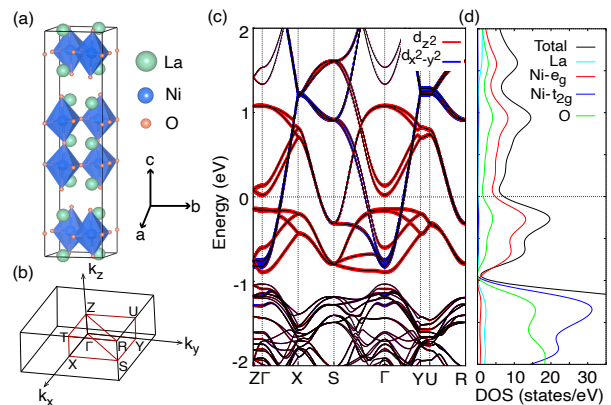


FIG. 1. (color online) The DFT electronic structures. (a) Schematic crystal structure of ultrathin films of $\text{La}_3\text{Ni}_2\text{O}_7$. (b) 3D BZ with high-symmetric points and lines marked which are obtained based on the real structural unit cell. (c) DFT+ U band structure of $\text{La}_3\text{Ni}_2\text{O}_7$ with $U = 3.5 \text{ eV}$, the blue solid line is Ni- $d_{x^2-y^2}$ orbital and the red one is Ni- d_{z^2} orbital. (d) The DOS of La, O and Ni-3d orbitals.

and Ni- d_{z^2} orbitals. As shown in Fig. S1 in the supplementary materials, the Wannier bands align remarkably well with the DFT bands near the Fermi level.

TB Model and Microscopic Hamiltonian: The DFT band structure shown in Fig. 1(c) exhibits a flat dispersion along the paths Z- Γ and Y-U, indicating the quasi-2D character of the band structure. Thus we only consider the hopping within a single-bilayer, and obtain the following TB Hamiltonian,

$$H_{\text{TB}} = \sum_{ij\mu\nu\alpha\beta\sigma} t_{i\mu\alpha,j\nu\beta} c_{i\mu\alpha\sigma}^\dagger c_{j\nu\beta\sigma} \quad (1)$$

Here i/j labels site, μ/ν labels combined layer and sublattice, α/β labels orbital (d_{z^2} (z) and $d_{x^2-y^2}$ (x)), σ labels the spin and $t_{i\mu\alpha,j\nu\beta}$ represents for the corresponding hopping integrals. The definition of the hopping parameters are illustrated in Fig. 2 and the corresponding values are listed in Table I. Note that in this pseudo-tetragonal *Amam* phase, each unit cell in the a - b plane consists of two sites A and B , as marked in Fig. 2(b). In comparison with the TB parameters for bulk $\text{La}_3\text{Ni}_2\text{O}_7$ at AP provided in Ref.[24], the intralayer nearest-neighbor hopping parameter of the $d_{x^2-y^2}$ electrons t_1^x listed in Table I becomes stronger due to the reduced in-plane lattice constant, while the interlayer hopping parameter of the d_{z^2} electrons t_1^z gets weaker due to the enhanced out-of-plane lattice constant. This character turns out to be crucial for the succeeding results.

The band structure of our eight-band TB model Eq. (1) is shown in Fig. 3(a), in comparison with the DFT one. Clearly, the former has captured the main features of the latter. The corresponding FS of this TB band structure is shown in Fig. 3(b), where there exist electron pockets α and γ centering around the Γ and X points and hole

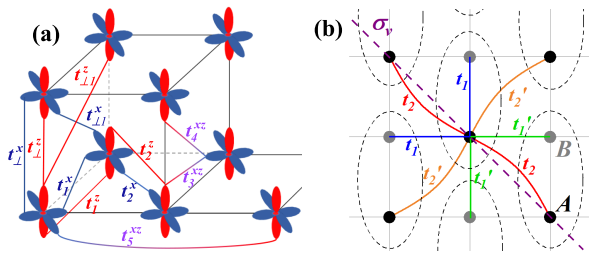


FIG. 2. (color online) Schematic of the hopping integrals for $\text{La}_3\text{Ni}_2\text{O}_7$ film. (a) Schematic of the main hopping integrals for the two-orbital bilayer TB model from side view, in which the third-nearest-neighbor hopping integrals (t_3^x and t_3^z in Tab. I) are not shown. Due to unit cell doubling in the *Amam* phase, each shown hopping integral in (a) can take different values labeled by t or t' in Tab. I according to the different locations of the two sites involved in the hopping displayed in (b). (b) Top view of the nearest-neighbor and next-nearest-neighbor hopping integrals in (a) for different locations of the two sites involved in the hopping. Each dashed oval represents a unit cell in the a - b plane consisting of A (black dot) and B (gray dot) sites. σ_v represents the mirror plane. Each $t_{1/2}$ or $t'_{1/2}$ shown in (b) indicates one of the hopping integrals exhibited in (a) according to the location of the involved bond.

TABLE I. The hopping integrals of the $(d_{z^2}, d_{x^2-y^2})$ -orbital bilayer TB model for the $\text{La}_3\text{Ni}_2\text{O}_7$ film. In the superscript and subscript, $x(z)$ represents the $d_{x^2-y^2}(d_{z^2})$ orbit, \perp represents interlayer hopping, and 1,2 represents the nearest-neighbor and next-nearest-neighbor hopping, respectively. ϵ is on-site energy. The symbol t or t' for each hopping integral means that this hopping integral can take different values according to the different locations of the two sites involved in the hopping exhibited in Fig. 2(b). The unit of all parameters is eV.

	t_1^x	t_2^x	t_3^x	t_\perp^x	t_\perp^{x1}
t	-0.456	0.071	-0.054	0	0
t'	-0.467	0.078			
	t_1^z	t_2^z	t_3^z	t_\perp^z	t_\perp^{z1}
t	-0.096	-0.013	-0.013	-0.541	0.027
t'	-0.087	-0.014			0.020
	t_3^{xz}	t_4^{xz}	t_5^{xz}	ϵ_x	ϵ_z
t	0.214	-0.035	-0.023	0.837	0
t'	0.210	-0.024			

pockets $\beta_{1,2}$ centering around the $X_{1,2}$ points, respectively. All of these pockets show mixing of orbital contents. We find nesting between the α pocket and the $\beta_{1,2}$ pockets with nesting vectors to be $\mathbf{Q} \approx (0, \pm 0.86\pi)$ and $\mathbf{Q}' \approx (\pm 0.86\pi, 0)$ in the folded BZ, respectively. Since the system has approximate C_4 rotational symmetry, the two nesting vectors are almost 90° -rotation related.

After considering the electron-electron interaction, we

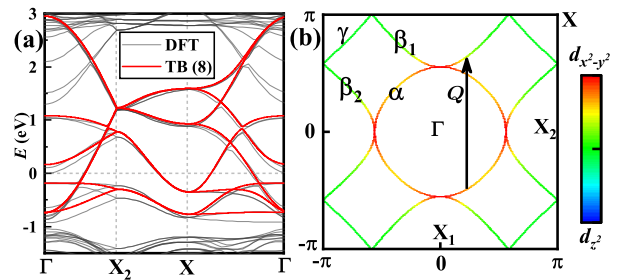


FIG. 3. (color online) Band structure and FSs of $\text{La}_3\text{Ni}_2\text{O}_7$ film at AP obtained from the eight-band TB-model Eq. (1). (a) The band structure of model Eq. (1) (red lines) along the high symmetry lines, compared with the DFT band structure (black lines). (b) FSs in the folded BZ, marked as α, β_1, β_2 and γ . The color in (b) indicates the orbital weight of $d_{x^2-y^2}$ and d_{z^2} . The FS-nesting vector is marked by \mathbf{Q} .

obtain the following multi-orbital Hubbard model,

$$\begin{aligned}
 H = & H_{\text{TB}} + U \sum_{i\mu\alpha} n_{i\mu\alpha\uparrow} n_{i\mu\alpha\downarrow} + V \sum_{i\mu} n_{i\mu z} n_{i\mu x} \\
 & + J_H \sum_{i\mu} \left[\left(\sum_{\sigma\sigma'} c_{i\mu z\sigma}^\dagger c_{i\mu x\sigma'}^\dagger c_{i\mu z\sigma'} c_{i\mu x\sigma} \right) \right. \\
 & \left. + \left(c_{i\mu z\uparrow}^\dagger c_{i\mu z\downarrow}^\dagger c_{i\mu x\downarrow} c_{i\mu x\uparrow} + \text{h.c.} \right) \right]. \quad (2)
 \end{aligned}$$

Here the U term is the intra-orbital repulsion, the V term is the inter-orbital repulsion and the J_H term is the Hund's coupling. We use the relation $U = V + 2J_H$ and set $J_H = U/6$ in our study.

The RPA Result: The Hamiltonian Eq. (2) is solved by standard multi-orbital RPA approach [92–98], introduced below. We calculate the renormalized spin (s) and charge (c) susceptibility matrix $\chi_{st}^{(s/c)pq}(\mathbf{q}, i\omega_n)$ up to the RPA level. Usually, the former dominates the latter for on-site Hubbard interactions. The maximal momentum \mathbf{Q} for the \mathbf{k} -space distribution of the spin susceptibility $\chi^{(s)}(\mathbf{q})$, defined as the largest eigenvalue of $\chi_{st}^{(s)pq}(\mathbf{q}, i\omega_n = 0)$, gives the wave vector of the characteristic spin fluctuations in the system. The eigenvector of $\chi_{st}^{(s)pq}(\mathbf{Q}, i\omega_n = 0)$ corresponding to its largest eigenvalue determines the spin fluctuation pattern within the unit cell. When U is beyond a critical interaction strength U_c , the spin susceptibility diverges, leading to spin-density-wave (SDW) order. For this system, we obtain $U_c = 1.13$ eV. For $U < U_c$, the short-range spin fluctuation mediates SC. The T_c is determined by the pairing eigenvalue λ through $T_c \sim e^{-1/\lambda}$, and the pairing symmetry is determined by the eigenvector of the linearized gap equation corresponding to the largest λ .

The distribution of the spin susceptibility $\chi^{(s)}(\mathbf{q})$ over the folded BZ is shown in Fig. 4(a), for $U = 1.05$ eV $< U_c$. This distribution is just maximized at the FS-nesting vector $\mathbf{Q} = (0, \pm 0.86\pi)$. Note that the other nesting

vector \mathbf{Q}' also provides a local maximum of the distribution with slightly lower value. The spin fluctuation pattern within the unit cell is illustrated in Fig. 4(b). This is an interlayer antiferromagnetic (AFM) pattern, in which both orbitals are significantly involved. The SDW phase difference between the two sublattices is $\theta \equiv \theta_A - \theta_B \approx 0.58\pi$, which is near the value of $\mathbf{Q}/2$ (here \mathbf{Q} is equally viewed as $2\pi - \mathbf{Q}$). The spin-fluctuation pattern over the lattice in one layer is illustrated in Fig. 4(c). For each orbital in each layer, the magnetic moment $m_{i\mu}$ at the μ ($=A$ or B) site in the i -th unit cell is given as $m_{i\mu} = m_0 \cos(\mathbf{Q} \cdot \mathbf{R}_i + \theta_\mu)$. This formula gives the unidirectional diagonal double-stripe pattern illustrated in Fig. 4(c), which is similar with the SDW ordered pattern detected in bulk $\text{La}_3\text{Ni}_2\text{O}_7$ at AP [99, 100]. Here Fig. 4(c) only illustrates the spin-fluctuation pattern.

We study the pairing symmetry for $U < U_c$. Fig. 4 (d) shows the U -dependent λ for the various leading pairing symmetries. In this approximate- D_4 -symmetric system, s -wave, p -wave and approximate- d -wave pairings are allowed. Fig. 4 (d) shows that the λ for these pairing symmetries enhance promptly with the enhancement of U for $U < U_c$. The leading and subleading pairing symmetries are the s -wave and approximate d_{xy} -wave for all the U parameters, respectively. The two pairing symmetries are nearly degenerate. In comparison with pressurized bulk $\text{La}_3\text{Ni}_2\text{O}_7$, the d_{xy} -wave pairing here becomes enhanced while the s -wave pairing gets weakened, because the combination of reduced in-plane lattice constant and enhanced out-plane one favors the intralayer-pairing d -wave state and suppresses the interlayer-pairing s -wave one. We also find that the leading λ here is lower than that of the pressurized bulk $\text{La}_3\text{Ni}_2\text{O}_7$, leading to lower T_c here, which is consistent with experiments.

Fig. 4 (e) and (f) show the distributions of the pairing gap functions of the leading s -wave and the subleading approximate d_{xy} -wave pairings on the FSs, respectively. In Fig. 4 (e), the gap sign of the α pocket is opposite to those of the $\beta_{1,2}$ and γ pockets, forming an s^\pm -wave pairing. In Fig. 4 (f), the gap function almost changes sign upon mirror reflection about the xz or the yz plane, leading to an approximate d_{xy} -wave pairing hosting gap nodes nearly on the x and y axes in the folded BZ. Note that this pairing symmetry is actually $d_{x^2-y^2}$ in the unfolded BZ corresponding to the undoubled pseudo-tetragonal unit cell. It is common for both pairing states that the gap functions on the Fermi patches connected by the nesting vector \mathbf{Q} or \mathbf{Q}' are different by a minus sign, which maximizes the energy gain from the superconducting condensation.

Discussion and Conclusion: Our results appeal for experimental verification. The band characters shown in Fig. 3 that the bonding- d_{z^2} band top is below the Fermi level and that there exists FS-nesting between the α and $\beta_{1,2}$ pockets can be verified by the angle-resolved-photoemission-spectrum. The interlayer AFM spin-fluctuation

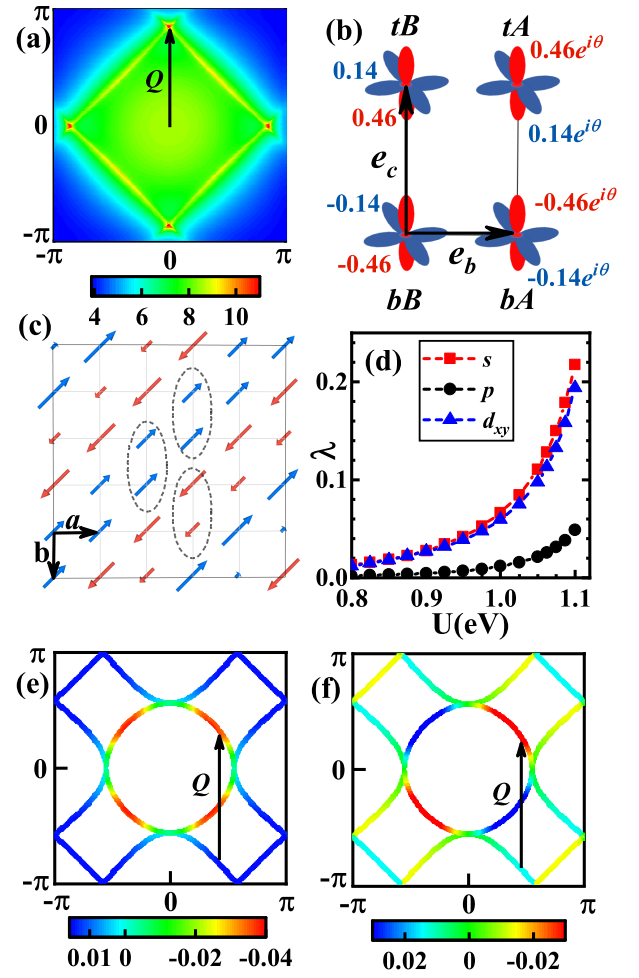


FIG. 4. (color online) (a) The distribution of the spin susceptibility $\chi^s(\mathbf{k})$ over the folded BZ for $U = 1.05$ eV. The maximal value of $\chi^s(\mathbf{k})$ just locates at $\mathbf{Q} \approx (0, \pm 0.86\pi)$. (b) The pattern of the spin fluctuation within a unit cell, in which red (blue) orbital represents the Ni- $3d_{z^2}$ ($3d_{x^2-y^2}$) orbital. The values are normalized. The difference between the SDW phases of the sublattice A and B within a unit cell is $\theta \approx 0.57\pi$. (c) Schematic spin-fluctuation pattern on the whole lattice within a layer. Each dashed oval represents a unit cell within a layer. The length and orientation/color of the arrows represent the magnitude and sign of the fluctuating magnetic moment $m_{i\alpha}$, respectively. (d) The largest pairing eigenvalue λ as function of U for different pairing symmetries. (e-f) Distributions of the leading s -wave and subleading approximate d_{xy} -wave pairing gap functions on the FSs for $U = 1.05$ eV. The FS-nesting vector is marked by \mathbf{Q} .

in the diagonal double-stripe pattern shown in Fig. 4(c) can be detected by the soft X-ray scattering experiment, although this spin pattern might only be short-ranged. The near degeneracy between the s^\pm -wave pairing and the d_{xy} -wave one might lead to formation of the $d_{xy} + is$ -wave pairing, which breaks the time-reversal symmetry and can be detected by such experiments as the μSR .

In conclusion, we have constructed a Ni-

$(3d_{z^2}, 3d_{x^2-y^2})$ -orbital TB model, which well fits the DFT band structure of the $\text{La}_3\text{Ni}_2\text{O}_7$ ultrathin film at AP. Our RPA calculations obtains an interlayer AFM spin fluctuation in the unidirectional diagonal double-stripe pattern similar with that detected in the bulk $\text{La}_3\text{Ni}_2\text{O}_7$ at AP. The leading pairing symmetries are nearly degenerate s^\pm -wave and approximate d_{xy} -wave pairings, caused by the reduced in-plane lattice constants and the enhanced out-of-plane one.

Acknowledgement

We are grateful to the stimulating discussions with Jia-Heng Ji and Ze-Yu Chen. F. Y. is supported by the National Natural Science Foundation of China (NSFC) under the Grant No. 12234016, and 12074031.

Appendix

We construct a Wannier model with the Ni- $d_{x^2-y^2}$ and Ni- d_{z^2} orbitals based on the maximally-localized Wannier function method, whose band structure is shown in Fig. S1.

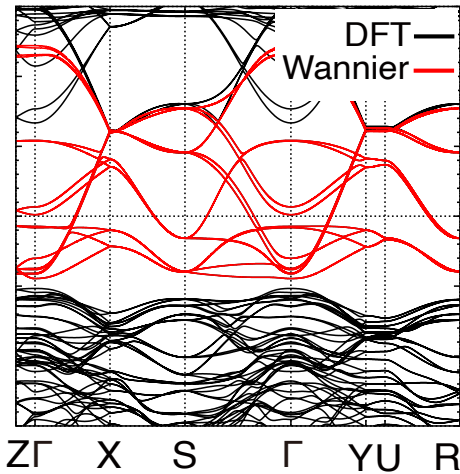


FIG. S1. (color online) Comparison of the DFT (black solid line) and Wannier band (red solid line) structures along a high symmetry path in the Brillouin zone.

* These two authors contributed equally to this work.

† minliu@buct.edu.cn

‡ yangfan_blg@bit.edu.cn

- [1] H. Sun, M. Huo, X. Hu, J. Li, Z. Liu, Y. Han, L. Tang, Z. Mao, P. Yang, B. Wang, J. Cheng, D.-X. Yao, G.-M. Zhang, and M. Wang, Signatures of superconductivity near 80 K in a nickelate under high pressure, *Nature* **621**, 493 (2023).

- [2] Y. Zhu, D. Peng, E. Zhang, B. Pan, X. Chen, L. Chen, H. Ren, F. Liu, Y. Hao, N. Li, *et al.*, Superconductivity in pressurized trilayer $\text{La}_4\text{Ni}_3\text{O}_{10-\delta}$ single crystals, *Nature* **631**, 531 (2024).
- [3] M. Zhang, C. Pei, X. Du, Y. Cao, Q. Wang, J. Wu, Y. Li, Y. Zhao, C. Li, W. Cao, *et al.*, Superconductivity in trilayer nickelate $\text{La}_4\text{Ni}_3\text{O}_{10}$ under pressure, [arXiv:2311.07423](https://arxiv.org/abs/2311.07423) (2023).
- [4] X. Huang, H. Zhang, J. Li, M. Huo, J. Chen, Z. Qiu, P. Ma, C. Huang, H. Sun, and M. Wang, Signature of superconductivity in pressurized trilayer-nickelate $\text{Pr}_4\text{Ni}_3\text{O}_{10-\delta}$, *Chin. Phys. Lett.* (2024).
- [5] Q. Li, Y.-J. Zhang, Z.-N. Xiang, Y. Zhang, X. Zhu, and H.-H. Wen, Signature of superconductivity in pressurized $\text{La}_4\text{Ni}_3\text{O}_{10}$, *Chin. Phys. Lett.* **41**, 017401 (2024).
- [6] Y. Zhang, D. Su, Y. Huang, Z. Shan, H. Sun, M. Huo, K. Ye, J. Zhang, Z. Yang, Y. Xu, Y. Su, R. Li, M. Smidman, M. Wang, L. Jiao, and H. Yuan, High-temperature superconductivity with zero resistance and strange-metal behaviour in $\text{La}_3\text{Ni}_2\text{O}_{7-\delta}$, *Nat. Phys.* **20**, 1269 (2024).
- [7] J. Hou, P.-T. Yang, Z.-Y. Liu, J.-Y. Li, P.-F. Shan, L. Ma, G. Wang, N.-N. Wang, H.-Z. Guo, J.-P. Sun, Y. Uwatoko, M. Wang, G.-M. Zhang, B.-S. Wang, and J.-G. Cheng, Emergence of high-temperature superconducting phase in pressurized $\text{La}_3\text{Ni}_2\text{O}_7$ crystals, *Chin. Phys. Lett.* **40**, 117302 (2023).
- [8] G. Wang, N. N. Wang, X. L. Shen, J. Hou, L. Ma, L. F. Shi, Z. A. Ren, Y. D. Gu, H. M. Ma, P. T. Yang, Z. Y. Liu, H. Z. Guo, J. P. Sun, G. M. Zhang, S. Calder, J.-Q. Yan, B. S. Wang, Y. Uwatoko, and J.-G. Cheng, Pressure-induced superconductivity in polycrystalline $\text{La}_3\text{Ni}_2\text{O}_7$, *Phys. Rev. X* **14**, 011040 (2024).
- [9] G. Wang, N. Wang, Y. Wang, L. Shi, X. Shen, J. Hou, H. Ma, P. Yang, Z. Liu, H. Zhang, X. Dong, J. Sun, B. Wang, K. Jiang, J. Hu, Y. Uwatoko, and J. Cheng, Observation of high-temperature superconductivity in the high-pressure tetragonal phase of $\text{La}_2\text{PrNi}_2\text{O}_{7-\delta}$, [arXiv:2311.08212](https://arxiv.org/abs/2311.08212) (2023).
- [10] M. Zhang, C. Pei, Q. Wang, Y. Zhao, C. Li, W. Cao, S. Zhu, J. Wu, and Y. Qi, Effects of pressure and doping on Ruddlesden-Popper phases $\text{La}_{n+1}\text{Ni}_n\text{O}_{3n+1}$, *J. Mater. Sci. Technol.* **185**, 147 (2024).
- [11] Y. Zhou, J. Guo, S. Cai, H. Sun, P. Wang, J. Zhao, J. Han, X. Chen, Q. Wu, Y. Ding, M. Wang, T. Xiang, H. Kwang Mao, and L. Sun, Investigations of key issues on the reproducibility of high- T_c superconductivity emerging from compressed $\text{La}_3\text{Ni}_2\text{O}_7$, [arXiv:2311.12361](https://arxiv.org/abs/2311.12361) (2023).
- [12] N. Wang, G. Wang, X. Shen, J. Hou, J. Luo, X. Ma, H. Yang, L. Shi, J. Dou, J. Feng, J. Yang, Y. Shi, Z. Ren, H. Ma, P. Yang, Z. Liu, Y. Liu, H. Zhang, X. Dong, Y. Wang, K. Jiang, J. Hu, S. Calder, J. Yan, J. Sun, B. Wang, R. Zhou, Y. Uwatoko, and J. Cheng, Bulk high-temperature superconductivity in the high-pressure tetragonal phase of bilayer $\text{La}_2\text{PrNi}_2\text{O}_7$, *Nature* **634**, 579 (2024).
- [13] J. Li, P. Ma, H. Zhang, X. Huang, C. Huang, M. Huo, D. Hu, Z. Dong, C. He, J. Liao, X. Chen, T. Xie, H. Sun, and M. Wang, Pressure-driven right-triangle shape superconductivity in bilayer nickelate $\text{La}_3\text{Ni}_2\text{O}_7$, [arXiv:2404.11369](https://arxiv.org/abs/2404.11369) (2024).
- [14] P. Puphal, P. Reiss, N. Enderlein, Y.-M. Wu, G. Khalullin, V. Sundaramurthy, T. Priessnitz, M. Knauft,

- A. Suthar, L. Richter, M. Isobe, P. A. van Aken, H. Takagi, B. Keimer, Y. E. Suyolcu, B. Wehinger, P. Hansmann, and M. Hepting, Unconventional crystal structure of the high-pressure superconductor $\text{La}_3\text{Ni}_2\text{O}_7$, *Phys. Rev. Lett.* **133**, 146002 (2024).
- [15] Z. Dong, M. Huo, J. Li, J. Li, P. Li, H. Sun, L. Gu, Y. Lu, M. Wang, Y. Wang, and Z. Chen, Visualization of oxygen vacancies and self-doped ligand holes in $\text{La}_3\text{Ni}_2\text{O}_{7-\delta}$, *Nature* **630**, 847 (2024).
- [16] X. Chen, J. Zhang, A. S. Thind, S. Sharma, H. LaBollita, G. Peterson, H. Zheng, D. P. Phelan, A. S. Botana, R. F. Klie, and J. F. Mitchell, Polymorphism in the Ruddlesden–Popper nickelate $\text{La}_3\text{Ni}_2\text{O}_7$: Discovery of a hidden phase with distinctive layer stacking, *J. Am. Chem. Soc.* **146**, 3640 (2024).
- [17] G. Wang, N. Wang, T. Lu, S. Calder, J. Yan, L. Shi, J. Hou, L. Ma, L. Zhang, J. Sun, B. Wang, S. Meng, M. Liu, and J. Cheng, Chemical versus physical pressure effects on the structure transition of bilayer nickelates, *arXiv:2408.09421* (2024).
- [18] Y. Li, X. Du, Y. Cao, C. Pei, M. Zhang, W. Zhao, K. Zhai, R. Xu, Z. Liu, Z. Li, J. Zhao, G. Li, Y. Qi, H. Guo, Y. Chen, and L. Yang, Electronic correlation and pseudogap-like behavior of high-temperature superconductor $\text{La}_3\text{Ni}_2\text{O}_7$, *Chin. Phys. Lett.* **41**, 087402 (2024).
- [19] M. Li, Y. Wang, C. Pei, M. Zhang, N. Li, J. Guan, M. Amboage, N.-D. Adama, Q. Kong, Y. Qi, and W. Yang, Distinguishing electronic band structure of single-layer and bilayer Ruddlesden–Popper nickelates probed by in-situ high pressure X-ray absorption near-edge spectroscopy, *arXiv:2410.04230* (2024).
- [20] X. Zhou, W. He, Z. Zhou, K. Ni, M. Huo, D. Hu, Y. Zhu, E. Zhang, Z. Jiang, S. Zhang, S. Su, J. Jiang, Y. Yan, Y. Wang, D. Shen, X. Liu, J. Zhao, M. Wang, M. Liu, Z. Du, and D. Feng, Revealing nanoscale structural phase separation in $\text{La}_3\text{Ni}_2\text{O}_{7-\delta}$ single crystal via scanning near-field optical microscopy, *arXiv:2410.06602* (2024).
- [21] T. Cui, S. Choi, T. Lin, C. Liu, G. Wang, N. Wang, S. Chen, H. Hong, D. Rong, Q. Wang, Q. Jin, J.-O. Wang, L. Gu, C. Ge, C. Wang, J. G. Cheng, Q. Zhang, L. Si, K. Juan Jin, and E.-J. Guo, Strain mediated phase crossover in Ruddlesden Popper nickelates, *Commun. Mater.* **5**, 32 (2024).
- [22] J. Yang, H. Sun, X. Hu, Y. Xie, T. Miao, H. Luo, H. Chen, B. Liang, W. Zhu, G. Qu, *et al.*, Orbital-dependent electron correlation in double-layer nickelate $\text{La}_3\text{Ni}_2\text{O}_7$, *Nat. Commun.* **15**, 4373 (2024).
- [23] L. Wang, Y. Li, S. Xie, F. Liu, H. Sun, C. Huang, Y. Gao, T. Nakagawa, B. Fu, B. Dong, Z. Cao, R. Yu, S. I. Kawaguchi, H. Kadobayashi, M. Wang, C. Jin, H. Kwang Mao, and H. Liu, Structure responsible for the superconducting state in $\text{La}_3\text{Ni}_2\text{O}_7$ at low temperature and high pressure conditions, *J. Am. Chem. Soc.* **146**, 7506 (2024).
- [24] Z. Huo, Z. Luo, P. Zhang, A. Yang, Z. Liu, X. Tao, Z. Zhang, S. Guo, Q. Jiang, W. Chen, D.-X. Yao, D. Duan, and T. Cui, Modulation of the octahedral structure and potential superconductivity of $\text{La}_3\text{Ni}_2\text{O}_7$ through strain engineering, *arXiv:2404.11001* (2024).
- [25] Y. Cao and Y.-f. Yang, Flat bands promoted by Hund’s rule coupling in the candidate double-layer high-temperature superconductor $\text{La}_3\text{Ni}_2\text{O}_7$ under high pressure, *Phys. Rev. B* **109**, L081105 (2024).
- [26] Q.-G. Yang, D. Wang, and Q.-H. Wang, Possible s_{\pm} -wave superconductivity in $\text{La}_3\text{Ni}_2\text{O}_7$, *Phys. Rev. B* **108**, L140505 (2023).
- [27] Y.-B. Liu, J.-W. Mei, F. Ye, W.-Q. Chen, and F. Yang, s^{\pm} -wave pairing and the destructive role of apical-oxygen deficiencies in $\text{La}_3\text{Ni}_2\text{O}_7$ under pressure, *Phys. Rev. Lett.* **131**, 236002 (2023).
- [28] C. Lu, Z. Pan, F. Yang, and C. Wu, Interlayer-coupling-driven high-temperature superconductivity in $\text{La}_3\text{Ni}_2\text{O}_7$ under pressure, *Phys. Rev. Lett.* **132**, 146002 (2024).
- [29] H. Oh and Y.-H. Zhang, Type-II t - J model and shared superexchange coupling from Hund’s rule in superconducting $\text{La}_3\text{Ni}_2\text{O}_7$, *Phys. Rev. B* **108**, 174511 (2023).
- [30] X.-Z. Qu, D.-W. Qu, J. Chen, C. Wu, F. Yang, W. Li, and G. Su, Bilayer t - J - J_{\perp} model and magnetically mediated pairing in the pressurized nickelate $\text{La}_3\text{Ni}_2\text{O}_7$, *Phys. Rev. Lett.* **132**, 036502 (2024).
- [31] Y.-F. Yang, G.-M. Zhang, and F.-C. Zhang, Interlayer valence bonds and two-component theory for high- T_c superconductivity of $\text{La}_3\text{Ni}_2\text{O}_7$ under pressure, *Phys. Rev. B* **108**, L201108 (2023).
- [32] K. Jiang, Z. Wang, and F.-C. Zhang, High temperature superconductivity in $\text{La}_3\text{Ni}_2\text{O}_7$, *Chin. Phys. Lett.* (2023).
- [33] Q. Qin and Y.-F. Yang, High- T_c superconductivity by mobilizing local spin singlets and possible route to higher T_c in pressurized $\text{La}_3\text{Ni}_2\text{O}_7$, *Phys. Rev. B* **108**, L140504 (2023).
- [34] J.-X. Zhang, H.-K. Zhang, Y.-Z. You, and Z.-Y. Weng, Strong pairing originated from an emergent \mathbb{Z}_2 berry phase in $\text{La}_3\text{Ni}_2\text{O}_7$, *Phys. Rev. Lett.* **133**, 126501 (2024).
- [35] Z. Pan, C. Lu, F. Yang, and C. Wu, Effect of rare-earth element substitution in superconducting $\text{R}_3\text{Ni}_2\text{O}_7$ under pressure, *Chin. Phys. Lett.* **41**, 087401 (2024).
- [36] H. Yang, H. Oh, and Y.-H. Zhang, Strong pairing from doping-induced feshbach resonance and second fermi liquid through doping a bilayer spin-one mott insulator: application to $\text{La}_3\text{Ni}_2\text{O}_7$, *Phys. Rev. B* **110**, 104517 (2024).
- [37] Z. Fan, J.-F. Zhang, B. Zhan, D. Lv, X.-Y. Jiang, B. Normand, and T. Xiang, Superconductivity in nickelate and cuprate superconductors with strong bilayer coupling, *Phys. Rev. B* **110**, 024514 (2024).
- [38] X. Wu, H. Yang, and Y.-H. Zhang, Deconfined fermi liquid to fermi liquid transition and superconducting instability, *Phys. Rev. B* **110**, 125122 (2024).
- [39] Y. Zhang, L.-F. Lin, A. Moreo, T. A. Maier, and E. Dagotto, Prediction of s^{\pm} -wave superconductivity enhanced by electronic doping in trilayer nickelates $\text{La}_4\text{Ni}_3\text{O}_{10}$ under pressure, *Phys. Rev. Lett.* **133**, 136001 (2024).
- [40] M. Zhang, H. Sun, Y.-B. Liu, Q. Liu, W.-Q. Chen, and F. Yang, The s^{\pm} -wave superconductivity in the pressurized $\text{La}_4\text{Ni}_3\text{O}_{10}$, *Phys. Rev. B* **110**, L180501 (2024).
- [41] Q.-G. Yang, K.-Y. Jiang, D. Wang, H.-Y. Lu, and Q.-H. Wang, Effective model and s_{\pm} -wave superconductivity in trilayer nickelate $\text{La}_4\text{Ni}_3\text{O}_{10}$, *Phys. Rev. B* **109**, L220506 (2024).
- [42] Y. Zhang, L.-F. Lin, A. Moreo, T. A. Maier, and E. Dagotto, Electronic structure, self-doping, and superconducting instability in the alternating single-layer trilayer stacking nickelates $\text{La}_3\text{Ni}_2\text{O}_7$, *Phys. Rev. B* **110**,

- L060510 (2024).
- [43] Y.-F. Yang, Decomposition of multilayer superconductivity with interlayer pairing, *Phys. Rev. B* **110**, 104507 (2024).
- [44] C. Lu, Z. Pan, F. Yang, and C. Wu, Interplay of two E_g orbitals in superconducting $\text{La}_3\text{Ni}_2\text{O}_7$ under pressure, *Phys. Rev. B* **110**, 094509 (2024).
- [45] Y. Shen, M. Qin, and G.-M. Zhang, Effective bilayer model hamiltonian and density-matrix renormalization group study for the high- T_c superconductivity $\text{La}_3\text{Ni}_2\text{O}_7$ under high pressure, *Chin. Phys. Lett.* **40**, 127401 (2023).
- [46] G. Heier, K. Park, and S. Y. Savrasov, Competing d_{xy} and s_{\pm} pairing symmetries in superconducting $\text{La}_3\text{Ni}_2\text{O}_7$: LDA + FLEX calculations, *Phys. Rev. B* **109**, 104508 (2024).
- [47] X. Sui, X. Han, X. Chen, L. Qiao, X. Shao, and B. Huang, Electronic properties of nickelate superconductor $\text{R}_3\text{Ni}_2\text{O}_7$ with oxygen vacancies, *Phys. Rev. B* **109**, 205156 (2024).
- [48] Z. Luo, X. Hu, M. Wang, W. Wú, and D.-X. Yao, Bilayer two-orbital model of $\text{La}_3\text{Ni}_2\text{O}_7$ under pressure, *Phys. Rev. Lett.* **131**, 126001 (2023).
- [49] Y. Zhang, L.-F. Lin, A. Moreo, and E. Dagotto, Electronic structure, dimer physics, orbital-selective behavior, and magnetic tendencies in the bilayer nickelate superconductor $\text{La}_3\text{Ni}_2\text{O}_7$ under pressure, *Phys. Rev. B* **108**, L180510 (2023).
- [50] Y. Zhang, L.-F. Lin, A. Moreo, T. A. Maier, and E. Dagotto, Structural phase transition, s_{\pm} -wave pairing, and magnetic stripe order in bilayered superconductor $\text{La}_3\text{Ni}_2\text{O}_7$ under pressure, *Nat. Commun.* **15**, 2470 (2024).
- [51] J. Huang, Z. D. Wang, and T. Zhou, Impurity and vortex states in the bilayer high-temperature superconductor $\text{La}_3\text{Ni}_2\text{O}_7$, *Phys. Rev. B* **108**, 174501 (2023).
- [52] B. Geisler, J. J. Hamlin, G. R. Stewart, R. G. Hennig, and P. Hirschfeld, Structural transitions, octahedral rotations, and electronic properties of $\text{A}_3\text{Ni}_2\text{O}_7$ rare-earth nickelates under high pressure, *npj Quantum Materials* **9**, 38 (2024).
- [53] L. C. Rhodes and P. Wahl, Structural routes to stabilize superconducting $\text{La}_3\text{Ni}_2\text{O}_7$ at ambient pressure, *Phys. Rev. Mater.* **8**, 044801 (2024).
- [54] Y. Zhang, L.-F. Lin, A. Moreo, T. A. Maier, and E. Dagotto, Electronic structure, magnetic correlations, and superconducting pairing in the reduced Ruddlesden-Popper bilayer $\text{La}_3\text{Ni}_2\text{O}_6$ under pressure: Different role of $d_{3z^2-r^2}$ orbital compared with $\text{La}_3\text{Ni}_2\text{O}_7$, *Phys. Rev. B* **109**, 045151 (2024).
- [55] N. Yuan, A. Elghandour, J. Arneth, K. Dey, and R. Klingeler, High-pressure crystal growth and investigation of the metal-to-metal transition of Ruddlesden-Popper trilayer nickelates $\text{La}_4\text{Ni}_3\text{O}_{10}$, *J. Cryst. Growth* **627**, 127511 (2024).
- [56] J. Li, C.-Q. Chen, C. Huang, Y. Han, M. Huo, X. Huang, P. Ma, Z. Qiu, J. Chen, X. Hu, L. Chen, T. Xie, B. Shen, H. Sun, D. Yao, and M. Wang, Structural transition, electric transport, and electronic structures in the compressed trilayer nickelate $\text{La}_4\text{Ni}_3\text{O}_{10}$, *Sci. China-Phys. Mech. Astron.* **67**, 117403 (2024).
- [57] B. Geisler, L. Fanfarillo, J. J. Hamlin, G. R. Stewart, R. G. Hennig, and P. Hirschfeld, Optical properties and electronic correlations in $\text{La}_3\text{Ni}_2\text{O}_{7-\delta}$ bilayer nickelates under high pressure, *npj Quantum Materials* **9**, 89 (2024).
- [58] H. Li, X. Zhou, T. Nummy, J. Zhang, V. Pardo, W. E. Pickett, J. F. Mitchell, and D. S. Dessau, Fermiology and electron dynamics of trilayer nickelate $\text{La}_4\text{Ni}_3\text{O}_{10}$, *Nat. Commun.* **8**, 704 (2017).
- [59] J.-X. Wang, Z. Ouyang, R.-Q. He, and Z.-Y. Lu, Non-fermi liquid and hund correlation in $\text{La}_4\text{Ni}_3\text{O}_{10}$ under high pressure, *Phys. Rev. B* **109**, 165140 (2024).
- [60] C.-Q. Chen, Z. Luo, M. Wang, W. Wú, and D.-X. Yao, Trilayer multiorbital models of $\text{La}_4\text{Ni}_3\text{O}_{10}$, *Phys. Rev. B* **110**, 014503 (2024).
- [61] F. Li, N. Guo, Q. Zheng, Y. Shen, S. Wang, Q. Cui, C. Liu, S. Wang, X. Tao, G.-M. Zhang, and J. Zhang, Design and synthesis of three-dimensional hybrid Ruddlesden-Popper nickelate single crystals, *Phys. Rev. Mater.* **8**, 053401 (2024).
- [62] F. Lechermann, J. Gondolf, S. Bötzel, and I. M. Eremin, Electronic correlations and superconducting instability in $\text{La}_3\text{Ni}_2\text{O}_7$ under high pressure, *Phys. Rev. B* **108**, L201121 (2023).
- [63] H. Sakakibara, N. Kitamine, M. Ochi, and K. Kuroki, Possible high T_c superconductivity in $\text{La}_3\text{Ni}_2\text{O}_7$ under high pressure through manifestation of a nearly half-filled bilayer Hubbard model, *Phys. Rev. Lett.* **132**, 106002 (2024).
- [64] Y. Gu, C. Le, Z. Yang, X. Wu, and J. Hu, Effective model and pairing tendency in bilayer Ni-based superconductor $\text{La}_3\text{Ni}_2\text{O}_7$, *arXiv:2306.07275* (2023).
- [65] Z. Liao, L. Chen, G. Duan, Y. Wang, C. Liu, R. Yu, and Q. Si, Electron correlations and superconductivity in $\text{La}_3\text{Ni}_2\text{O}_7$ under pressure tuning, *Phys. Rev. B* **108**, 214522 (2023).
- [66] Y. Zhang, L.-F. Lin, A. Moreo, T. A. Maier, and E. Dagotto, Trends in electronic structures and s_{\pm} -wave pairing for the rare-earth series in bilayer nickelate superconductor $\text{R}_3\text{Ni}_2\text{O}_7$, *Phys. Rev. B* **108**, 165141 (2023).
- [67] Y.-H. Tian, Y. Chen, J.-M. Wang, R.-Q. He, and Z.-Y. Lu, Correlation effects and concomitant two-orbital s_{\pm} -wave superconductivity in $\text{La}_3\text{Ni}_2\text{O}_7$ under high pressure, *Phys. Rev. B* **109**, 165154 (2024).
- [68] R. Jiang, J. Hou, Z. Fan, Z.-J. Lang, and W. Ku, Pressure driven fractionalization of ionic spins results in cupratelike high- T_c superconductivity in $\text{La}_3\text{Ni}_2\text{O}_7$, *Phys. Rev. Lett.* **132**, 126503 (2024).
- [69] D.-C. Lu, M. Li, Z.-Y. Zeng, W. Hou, J. Wang, F. Yang, and Y.-Z. You, Superconductivity from doping symmetric mass generation insulators: Application to $\text{La}_3\text{Ni}_2\text{O}_7$ under pressure, *arXiv:2308.11195* (2023).
- [70] N. Kitamine, M. Ochi, and K. Kuroki, Theoretical designing of multiband nickelate and palladate superconductors with $d^{8+\delta}$ configuration, *arXiv:2308.12750* (2023).
- [71] Z. Luo, B. Lv, M. Wang, W. Wú, and D.-X. Yao, High- T_c superconductivity in $\text{La}_3\text{Ni}_2\text{O}_7$ based on the bilayer two-orbital t-J model, *npj Quantum Materials* **9**, 61 (2024).
- [72] H. Sakakibara, M. Ochi, H. Nagata, Y. Ueki, H. Sakurai, R. Matsumoto, K. Terashima, K. Hirose, H. Ohta, M. Kato, Y. Takano, and K. Kuroki, Theoretical analysis on the possibility of superconductivity in the trilayer Ruddlesden-Popper nickelate $\text{La}_4\text{Ni}_3\text{O}_{10}$ under pressure and its experimental examination: Comparison with

- La₃Ni₂O₇, *Phys. Rev. B* **109**, 144511 (2024).
- [73] H. Lange, L. Homeier, E. Demler, U. Schollwöck, A. Bohrdt, and F. Grusdt, Pairing dome from an emergent feshbach resonance in a strongly repulsive bilayer model, *Phys. Rev. B* **110**, L081113 (2024).
- [74] H. Lange, L. Homeier, E. Demler, U. Schollwöck, F. Grusdt, and A. Bohrdt, Feshbach resonance in a strongly repulsive bilayer model: a possible scenario for bilayer nickelate superconductors, [arXiv:2309.15843](https://arxiv.org/abs/2309.15843) (2023).
- [75] T. Kaneko, H. Sakakibara, M. Ochi, and K. Kuroki, Pair correlations in the two-orbital hubbard ladder: Implications for superconductivity in the bilayer nickelate La₃Ni₂O₇, *Phys. Rev. B* **109**, 045154 (2024).
- [76] S. Rye, N. Witt, and T. O. Wehling, Quenched pair breaking by interlayer correlations as a key to superconductivity in La₃Ni₂O₇, *Phys. Rev. Lett.* **133**, 096002 (2024).
- [77] Z. Ouyang, M. Gao, and Z.-Y. Lu, Absence of electron-phonon coupling superconductivity in the bilayer phase of La₃Ni₂O₇ under pressure, *npj Quantum Materials* **9**, 80 (2024).
- [78] V. Christiansson, F. Petocchi, and P. Werner, Correlated electronic structure of La₃Ni₂O₇ under pressure, *Phys. Rev. Lett.* **131**, 206501 (2023).
- [79] D. A. Shilenko and I. V. Leonov, Correlated electronic structure, orbital-selective behavior, and magnetic correlations in double-layer La₃Ni₂O₇ under pressure, *Phys. Rev. B* **108**, 125105 (2023).
- [80] W. Wú, Z. Luo, D.-X. Yao, and M. Wang, Superexchange and charge transfer in the nickelate superconductor La₃Ni₂O₇ under pressure, *Sci. China-Phys. Mech. Astron.* **67**, 117402 (2024).
- [81] X. Chen, P. Jiang, J. Li, Z. Zhong, and Y. Lu, Critical charge and spin instabilities in superconducting La₃Ni₂O₇, [arXiv:2307.07154](https://arxiv.org/abs/2307.07154) (2023).
- [82] Z. Ouyang, J.-M. Wang, J.-X. Wang, R.-Q. He, L. Huang, and Z.-Y. Lu, Hund electronic correlation in La₃Ni₂O₇ under high pressure, *Phys. Rev. B* **109**, 115114 (2024).
- [83] Y. Wang, K. Jiang, Z. Wang, F.-C. Zhang, and J. Hu, Electronic and magnetic structures of bilayer La₃Ni₂O₇ at ambient pressure, *Phys. Rev. B* **110**, 205122 (2024).
- [84] S. Bötzel, F. Lechermann, J. Gondolf, and I. M. Eremin, Theory of magnetic excitations in multilayer nickelate superconductor La₃Ni₂O₇, *Phys. Rev. B* **109**, L180502 (2024).
- [85] E. K. Ko, Y. Yu, Y. Liu, L. Bhatt, J. Li, V. Thampy, C.-T. Kuo, B. Y. Wang, Y. Lee, K. Lee, J.-S. Lee, B. H. Goodge, D. A. Muller, and H. Y. Hwang, Signatures of ambient pressure superconductivity in thin film La₃Ni₂O₇, *Nature* [10.1038/s41586-024-08525-3](https://doi.org/10.1038/s41586-024-08525-3) (2024).
- [86] G. Zhou, W. Lv, H. Wang, Z. Nie, Y. Chen, Y. Li, H. Huang, W. Chen, Y. Sun, Q.-K. Xue, and Z. Chen, Ambient-pressure superconductivity onset above 40 K in bilayer nickelate ultrathin films, [arXiv:2312.16622](https://arxiv.org/abs/2312.16622) (2024).
- [87] G. Kresse and J. Hafner, Ab initio molecular dynamics for liquid metals, *Phys. Rev. B* **47**, 558 (1993).
- [88] G. Kresse and J. Furthmüller, Efficient iterative schemes for ab initio total-energy calculations using a plane-wave basis set, *Phys. Rev. B* **54**, 11169 (1996).
- [89] P. E. Blöchl, Projector augmented-wave method, *Phys. Rev. B* **50**, 17953 (1994).
- [90] J. P. Perdew, K. Burke, and M. Ernzerhof, Generalized gradient approximation made simple, *Phys. Rev. Lett.* **77**, 3865 (1996).
- [91] A. A. Mostofi, J. R. Yates, Y.-S. Lee, I. Souza, D. Vanderbilt, and N. Marzari, wannier90: A tool for obtaining maximally-localised wannier functions, *Comput. Phys. Commun.* **178**, 685 (2008).
- [92] T. Takimoto, T. Hotta, and K. Ueda, Strong-coupling theory of superconductivity in a degenerate hubbard model, *Phys. Rev. B* **69**, 104504 (2004).
- [93] K. Yada and H. Kontani, Origin of weak pseudogap behaviors in Na_{0.35}CoO₂: Absence of small hole pockets, *J. Phys. Soc. Jpn.* **74**, 2161 (2005).
- [94] K. Kubo, Pairing symmetry in a two-orbital hubbard model on a square lattice, *Phys. Rev. B* **75**, 224509 (2007).
- [95] S. Graser, T. Maier, P. Hirschfeld, and D. Scalapino, Near-degeneracy of several pairing channels in multi-orbital models for the Fe pnictides, *New J. Phys.* **11**, 025016 (2009).
- [96] F. Liu, C.-C. Liu, K. Wu, F. Yang, and Y. Yao, $d + id'$ chiral superconductivity in bilayer silicene, *Phys. Rev. Lett.* **111**, 066804 (2013).
- [97] M. Zhang, J.-J. Hao, X. Wu, and F. Yang, Lifshitz transition enhanced triplet p_z -wave superconductivity in hydrogen-doped KCr₃As₃, *Phys. Rev. B* **105**, 134509 (2022).
- [98] K. Kuroki, S. Onari, R. Arita, *et al.*, Unconventional pairing originating from the disconnected fermi surfaces of superconducting LaFeAsO_{1-x}F_x, *Phys. Rev. Lett.* **101** (2008).
- [99] X. Chen, J. Choi, Z. Jiang, J. Mei, K. Jiang, J. Li, S. Agrestini, M. Garcia-Fernandez, X. Huang, H. Sun, D. Shen, M. Wang, J. Hu, Y. Lu, K.-J. Zhou, and D. Feng, Electronic and magnetic excitations in La₃Ni₂O₇, *Nat. Commun.* **15**, 9597 (2024).
- [100] N. K. Gupta, R. Gong, Y. Wu, M. Kang, C. T. Parzyck, B. Z. Gregory, N. Costa, R. Sutarto, S. Sarker, A. Singer, D. G. Schlom, K. M. Shen, and D. G. Hawthorn, Anisotropic spin stripe domains in bilayer La₃Ni₂O₇, [arXiv:2409.03210](https://arxiv.org/abs/2409.03210) (2024).